12M-0044

A Physics-Based Vehicle/Terrain Interaction Model for Soft Soil Off-Road Vehicle Simulations

Justin Madsen, Andrew Seidl, Dan Negrut, Paul Ayers, George Bozdech, Jeff Freeman, James O'Kins, Al Reid (Do NOT enter this information. It will be pulled from participant tab in MyTechZone)

Affiliation (Do NOT enter this information. It will be pulled from participant tab in MyTechZone)

ABSTRACT

In the context of off-road vehicle simulations, deformable terrain models mostly fall into three categories: simple visualization of an assumed terrain deformation, use of empirical relationships for the deformation, or finite/discrete element approaches for the terrain. A real-time vehicle dynamics simulation with a physics-based tire model (brush, beam-based or Finite Element models) requires a terrain model that accurately reflects the deformation and response of the soil to all possible inputs of the tire in order to correctly simulate the response of the vehicle. The real-time requirement makes complex finite/discrete element approaches unfeasible, and the use of a ring or beam -based tire model excludes purely empirical terrain models.

We present the development of a three-dimensional vehicle/terrain interaction model which is comprised of a tire and deformable terrain model to be used with a real-time vehicle dynamics simulator. The governing equations of both models are physics-based, rather than utilizing popular terramechanics models that are empirical. The tire draws on a lumped-mass model based on a radial spring-damper-mass distribution. The terrain model utilizes Boussinesq and Cerruti soil mechanics equations to determine the pressure distribution and deformation of a volume of soil as a function of normal and tangent forces applied at the soil surface by the tire. The soil volume that describes the terrain is discretized as a set of vertical columns of soil, and the deformation of each is modeled using visco-elasto-plastic compressibility relationships that relate subsoil pressures to a change in bulk density of the soil, which in turn produces soil displacements. Different loading combinations applied by a tire passing over a column of soil will be reflected in the state of each volume of soil contained in the column, rather than treating the column of soil as homogeneous in the vertical direction and only associating one set of parameters with the entire column, e.g. a Bekker type model. Furthermore, the time-dependent elastic and plastic response of the soil to repetitive compression/rebound tire loads is also taken into account. Horizontal soil force/displacement produced by tractive and turning forces will also be incorporated into the model. Both the vertical and horizontal force/displacement relationships allow the calculation of total energy and power required to deform the terrain. These physics-based models will be integrated into a real-time vehicle dynamics simulator and is anticipated to lead to a realistic vehicle dynamic response when driving on off-road, deformable terrain conditions, especially when repeated loading occurs or non-homogeneous soil conditions are present. Additionally, the changes in soil states can be used to directly compute the energy and power required to deform the terrain. In order to retain the ability to run real-time simulations, a GPU-accelerated approach is considered to leverage the inherently parallel nature of performing multiple independent terrain geometry queries and soil-mechanics calculations. Numerical experiments include a single soil volume node under a known load and a simplified tire model applying normal forces on the surface of the terrain. Results are given for the vertical plastic soil deformation, and for the power and energy required to perform the deformations.

INTRODUCTION

We present the development of vehicle/terrain interaction model to be used with an existing real-time driving simulator at the US Army's Tank Automotive Research, Development and Engineering Center (TARDEC). The model will make use of existing simulation tools and terrain profile measurement information as additional requirements to the development. The US Army TARDEC ride-simulator (Richmond, 2004) is comprised of a multibody dynamics vehicle model that is interfaced with an empirically-based deformable terrain model. The terrain model is able to query lateral and longitudinal location points on a terrain database which returns various terrain information about a data point, notably the undisturbed terrain height, the change in height, the Rating Cone-Index (RCI), and the type of terrain, e.g. soil classification code. Geometry associated with the terrain profile is a combination of low-

Report Documentation Page

Form Approved
OMB No. 0704-0188

1. REPORT DATE	2. REPORT TYPE	3. DATES COVERED
19 DEC 2011	**Journal Article**	**10-06-2011 to 19-10-2011**

4. TITLE AND SUBTITLE
A Physics Based Vehicle Terrain Interaction Model for Soft Soil off-Road Vehicle Simulations

5a. CONTRACT NUMBER
5b. GRANT NUMBER
5c. PROGRAM ELEMENT NUMBER

6. AUTHOR(S)
Justin Madsen; Andrew Seidl; Dan Negrut; James O' Kins; Al Reid

5d. PROJECT NUMBER
5e. TASK NUMBER
5f. WORK UNIT NUMBER

7. PERFORMING ORGANIZATION NAME(S) AND ADDRESS(ES)
Department of Mechanical Engineering,University of Wisconsin - Madison,500 Lincoln Dr,Madison,Wi,53706

8. PERFORMING ORGANIZATION REPORT NUMBER
; #22501

9. SPONSORING/MONITORING AGENCY NAME(S) AND ADDRESS(ES)
U.S. Army TARDEC, 6501 East Eleven Mile Rd, Warren, Mi, 48397-5000

10. SPONSOR/MONITOR'S ACRONYM(S)
TARDEC

11. SPONSOR/MONITOR'S REPORT NUMBER(S)
#22501

12. DISTRIBUTION/AVAILABILITY STATEMENT
Approved for public release; distribution unlimited

13. SUPPLEMENTARY NOTES
Submitted to 2012 SAE International

14. ABSTRACT
In the context of off-road vehicle simulations, deformable terrain models mostly fall into three categories: simple visualization of an assumed terrain deformation, use of empirical relationships for the deformation, or finite/discrete element approaches for the terrain. A real-time vehicle dynamics simulation with a physics-based tire model (brush, beam-based or Finite Element models) requires a terrain model that accurately reflects the deformation and response of the soil to all possible inputs of the tire in order to correctly simulate the response of the vehicle. The real-time requirement makes complex finite/discrete element approaches unfeasible, and the use of a ring or beam -based tire model excludes purely empirical terrain models.

15. SUBJECT TERMS

16. SECURITY CLASSIFICATION OF:			17. LIMITATION OF ABSTRACT	18. NUMBER OF PAGES	19a. NAME OF RESPONSIBLE PERSON
a. REPORT	b. ABSTRACT	c. THIS PAGE			
unclassified	**unclassified**	**unclassified**	**Public Release**	**14**	

fidelity terrain height measurements with superimposed NURBS for high-frequency content (Morrison 2004), and an example terrain profile is shown in Figure 1. This information is used with empirical relations developed at the Engineer, Research and Development Center (ERDC) to estimate the terrain sinkage and vehicle tractive forces under a given tire loading condition. The interaction forces at the tire/terrain interface, which are responsible for soil deformation, are then resolved as tire-spindle forces and are passed back to the vehicle model. This approach, based on empirical terramechanics relations makes several assumptions such as, for instance, the premise of equally distributed pressure under the tire footprint. The tire is assumed to be rigid, and furthermore, the soil mechanics are based on static whole wheel approximated as a function of vehicle speed, which leads to inaccurate results for a slow moving or rapidly accelerating/decelerating vehicle.

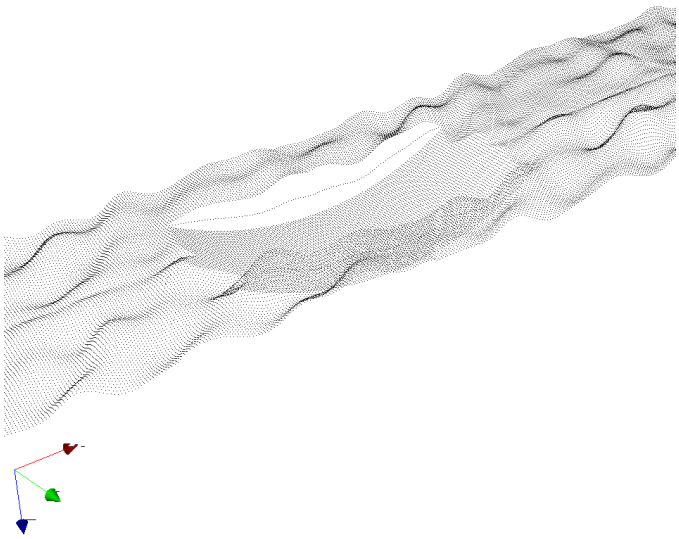

Figure 1 Terrain geometry as a heightmap, after an applied displacement

The principle behind the new Vehicle/Terrain Interaction Model (VTIM) is that the governing equations of the model are physics-based, instead of the current empirical model. The inputs to the model consist of vehicle parameters and operating conditions. The outputs include terrain deformation, vehicle power/energy requirements and tire forces. The new VTIM builds around three components: (i) a surface loading mechanism due to a non-rigid tire, (ii) a rigorous vertical soil stress/strain integration, and (iii) lateral soil force/displacement characterization due to soil surface shear and bulldozing forces. They rely on physics-based tire and terrain models and will be integrated into the existing vehicle model and terrain database system.

The soil mechanics equations developed result in smooth, continuous functions over the affected volume of soil for both vertical and horizontal soil deformation; however, the database will discretize these values into a three dimensional grid under the affected area for database storage purposes and to maintain the ability to run real-time simulations. The dimension and number of elements in this grid will be tailored to retain the accuracy of the original, continuous functions. Multiple vertical and horizontal forces will be applied on the terrain surface, depending on the number of tire nodes in contact with the terrain. The total horizontal and vertical pressure for each soil node is determined by superimposing the contribution from each tire force that causes subsoil stress on the particular soil node. Vertical sinkage and the soil states for each soil node are calculated and used to update the terrain database for the next time step. They are subsequently used in an energy/power analysis that gauges the mobility and the associated power requirements of the vehicle.

In the proposed approach real-time simulations will be possible due to the inherent parallel nature of the tire node terrain queries, which will utilize GPU hardware to accelerate the computation of the soil mechanics response. The single-instruction-multiple-data programming model promoted by GPU accelerators will also be leveraged for tire forces and soil-mechanics calculations due to the node-based approach adopted in the proposed methodology.

VEHICLE TERRAIN INTERACTION MODEL COMPONENTS

This section contains the physics-based models that will replace the existing empirical components used in the real-time off-road vehicle dynamics simulator at US Army TARDEC. No changes are made to the vehicle model, which is already a multibody

dynamics-based model. The tire model is presented, followed by the soil mechanics model, which is broken down into its constitutive parts with an in-depth discussion of each component.

TIRE MODEL DESCRIPTION

In order to enable real-time simulation, the tire and soil models are decoupled. The spring-damper tire model combines a series of lumped masses, linked to each other and the wheel rim using discrete spring-damper elements. The model consists of two components, which were detailed for hard surfaces in Negrut and Freeman (1994). The first component is the model shown in Figure 2, which incorporates both radial springs and dampers, and interradial springs. The second component is the tire tread discretized into a number of lumped masses. Lumped masses are connected to each other and to the wheel rim using tangential and lateral spring elements. The numerical results presented in this work do not contain tire dynamics, thus the lumped mass tire tread description is excluded, but can be found in the literature.

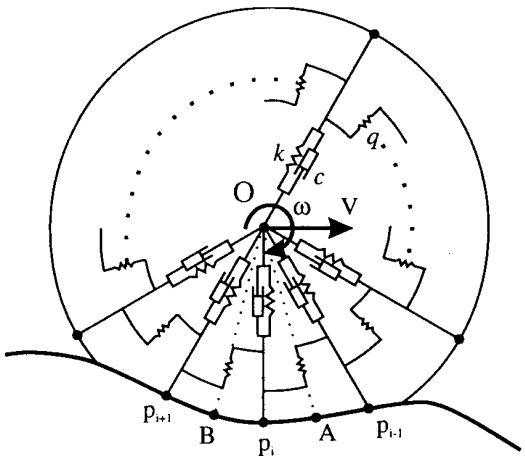

Figure 2 Radial-interradial spring-damper tire model

Each of the spring-damper elements composing the rolling radial-interradial model can either be an active element, in contact with the ground and queried using the terrain geometry database, or a passive element. In order to determine the active elements, the terrain geometry is queried for each lumped mass coordinate tuple, $r_i = \{x_i \quad y_i \quad z_i\}^T$. If there is penetration of the terrain geometry, then the length of the spring-damper element is calculated as

$$\ell_i = \sqrt{\left(r_i' - r_c\right)^T \left(r_i' - r_c\right)} \tag{1}$$

where r_i' is the coordinate of P_i, the i^{th} terrain contact point, and r_c is the coordinate of the center of the wheel, both expressed in global coordinates. For each active element, a Boolean activity array will be set to true (1), while for each passive element, the activity array will be set to false (0). Based on wheel rotational speed, the array will be used to minimize the number of terrain queries at each timestep.

The radial force acting on the i^{th} mass element can then be expressed as

$$F_i = k\left(R - \ell_i\right) + q\left(\ell_{i+1} - \ell_i\right) + q\left(\ell_{i-1} - \ell_i\right) - c\dot{\ell}_i \tag{2}$$

where k and q are the stiffness of the radial and interradial springs, c is the radial damping, and R is the undeformed radius of the tire. For the undeformed elements, the force F_i is zero.

SOIL MECHANICS MODELS

The physics-based soil mechanics model, developed by Ayers and Bozdech, is a combination of many different models and is the most substantial theory contribution to the project. As such, this section is broken into its constitutive parts, which include: vertical stress and sinkage, repeated loading effects, shear stress/shear displacement effects. Power and energy calculations for both vertical and horizontal soil deformations are also included.

Vertical Visco-Elasto-Plastic Model

As the soil surface contact area and the vehicle normal surface loads are known, the subsurface stress distribution needs to be determined. The method for calculating the stress in a semi-infinite, homogeneous, isotropic, elastic medium subject to a vertical point load applied on the surface was first developed by Boussinesq (Wong, 2001):

$$\sigma_z = \frac{3}{2\pi} \frac{1}{[1+(r/z)^2]^{5/2}} \frac{W}{z^2} \tag{3}$$

where σ_z is the stress at the depth z, W is the point load, and r is the horizontal distance from the point load to the point in equation. When the Boussinesq model is applied for soil, there is a tendency for the compressive stress in the soil to concentrate around the loading axis. This tendency becomes greater when the soil becomes more plastic due to increased moisture content or when the soil is less cohesive, such as sand. In view of this phenomenon, Frohlich introduced a concentration factor ν to Boussinesq's equations, for hard soil, $\nu = 3$, for normal soil $\nu = 4$, and for soft soil, $\nu = 5$ (Koolen and Kuipers, 1983). Other literature employs concentration factors for hard soil, $\nu = 4$, for normal soil, $\nu = 5$, and for soft soil, $\nu = 6$ (Ayers, 1991; Wong, 2001). The concentration factor has been assumed to vary with the current soil density, the minimum density, and the maximum density of the soil material (Binger and Wells, 1989). An equation was developed to calculate the value of concentration factor.

$$\nu = 6 + (6-4)(P - P_{\min}) / (P_{\min} - P_{\max}) \tag{4}$$

where ν is the concentration factor, P is the current dry bulk density of the soil (g/cm^3), $P_{\max}$ is the maximum dry bulk density of the soil (g/cm^3), and $P_{\min}$ is the minimum dry bulk density of the soil (g/cm^3). Introducing the concentration factor, the vertical stress under the plate can be expressed in Cartesian coordinates as (Ayers and Riper, 1991):

$$\sigma_z = \frac{\nu W z^{\nu}}{2\pi (r^2 + z^2)^{(\nu/2+1)}} \tag{5}$$

After the subsurface stress distribution is determined, soil strain (or compaction) is based on soil visco-elasto-plastic relationships. These relationships are to be defined for the USCS terrain described in the terrain database. The constitutive (stress/strain) relationships for these soils are needed to define the soil response (sinkage) due to loading.

If bulk density, ρ, is plotted vs. $\log_{10}$ applied stress, σ_a, the relationship will be linear. During the compression procedure, soil particles will be rearranged and brought closer together. The straight line is also called the virgin compression curve, VCC, and the slope of that line is called the compression index, C (Larson et al., 1980). If the soil has previously been subjected to a stress and a further stress is applied, the bulk density-stress relationship will increase along a line with a slight slope (secondary compression) until it joins with the VCC curve. The linear portion of the VCC in Figure 3 can be described by (Larson et al., 1980)

$$\rho = \rho_k + C \log_{10} \left(\sigma_a / \sigma_k \right), \tag{6}$$

where ρ is the computed bulk density, ρ_k is the density at a known stress σ_k, σ_a is the applied normal stress, and C is the slope of the line. If the VCC represents a dry soil, lines for soils at water contents less than saturation will be shifted to the left and parallel to the dry soil line. If the relationship in Eq. (6) is known for a given water content, or degree of water saturation, S_k, curves for other water contents can be computed from the following relationship (Larson et al., 1980):

$$\rho = \left[\rho_k + S_T \left(S_1 - S_k \right) \right] + C \log_{10} \left(\sigma_a / \sigma_k \right) \tag{7}$$

where S_T is the slope of the bulk density vs. degree of water saturation curve at a given stress, and S_1 is the desired degree of saturation. By predicting the bulk density variation due to repetitive normal loading, the soil element's vertical displacement can be determined along with the related net energy and power that must be applied to the mass. A soil element with a given height (H) has a vertical displacement (z) expressed by the following equation:

$$z = \left(1 - \left(\rho_0 / \rho_1 \right)\right) \cdot H \tag{8}$$

where ρ_0 is the initial bulk density and ρ_1 is the final bulk density.

Power and Energy Calculations

Positive soil element vertical displacement occurs during compression when ρ_1 exceeds ρ_0 in Eq. (8). The required energy (E) to displace the soil element vertically (Δz) is calculated by the following equation:

$$E = F \cdot \Delta z = (\sigma \cdot A) \cdot \Delta z \tag{9}$$

where σ is the sub-surface normal stress, A is the soil element cross-sectional area in the horizontal plane.

Equation (9) is only applied in the model during compression (i.e. positive Δz). E is assumed to remain constant during rebound because the energy lost by the soil element is assumed to be negligible in the model. The power required during compression of the soil element in a given time interval (Δt) is determined by the following:

$$P = E / \Delta t \tag{10}$$

P is nonzero only when compression of the soil element occurs.

Repeated Vertical Loading

The time-dependent elastic and plastic properties of the soil are needed to fully describe the soil response to tire/track loads. Rebound properties are defined by the soil rebound index or measure of the decrease in density as the applied load is released. The time-dependent or viscous soil properties can be defined using a time constant of soil deformation.

The compression and rebound time constants, τ_c and τ_r, must be defined for the soil element and the values are indicators of the time required for the dependent variable ρ to change from the initial to the final value during compression and rebound. The following is the general form of the time-dependent compression and rebound factor of the model, respectively:

$$\left(1 - e^{t/\tau_c}\right), \quad \left(1 - e^{t/\tau_r}\right) \tag{11}$$

During compression, the change in bulk density is calculated by multiplying the theoretical change in bulk density determined from Eq. (7) by the time-dependent compression factor from the above expression. By doing so, the effect of the duration that a given normal load being exerted on the soil element is accounted for in the model. If a vehicle travels at a slower rate, the normal load is applied over a longer period of time; thus, the bulk density increase should be greater at a lower travel speeds. The time-dependent factor attempts to account for the time-dependent nature of a soil element's response to an applied normal load.

The rebound constant must also be predicted for the soil element. The value of the rebound constant is the amount of rebound that occurs when the calculated bulk density associated with the applied normal stress is less than the current density. If the bulk density increase is less than the rebound constant multiplied by two, the magnitude of the rebound in the model is estimated as half of the bulk density increase during compression. The rebound that occurs in a given time interval is also calculated by multiplying the time-

dependent factor from above by the net rebound where *t* is equal to zero when compression of the soil element ends and rebound begins.

Lateral/Longitudinal Shear Stress/Deformation Model

To produce mobility, tractive tire forces must be supported by the soil. These forces produce wheel or track slip and produce additional soil deformation. The ability of the soil to support tractive forces can best be described by both the soil shear strength parameters (cohesion and friction angle) and the soil shear deformation modulus (describes the shear stress/deformation relationship of the soil).Both longitudinal and lateral horizontal shear forces are known to produce vertical subsurface stresses, resulting in increased vehicle sinkage, and the phenomenon is known as "slip sinkage". Field and laboratory tests of turning vehicles have shown that lateral stresses produce lateral displacement and increased sinkage. This additional sinkage is considered "slide sinkage".

The method for calculating the vertical stress in a semi-infinite, homogeneous, isotropic, elastic medium subject to a horizontal point load applied on the surface was first developed by Cerruti (Feda, 1978):

$$\sigma_z = \frac{3}{2\pi} \frac{r(\cos\Theta)}{[1+(r/z)^2]^{5/2}} \frac{H}{z^3} \tag{12}$$

where σ_z is the vertical stress at the depth z, H is the horizontal force, Θ is the angle between the applied force direction and the direction to the location of the vertical stress, and r is the horizontal distance from the point load to the location of the vertical stress. These horizontal load induced vertical stresses will be added to the vertical stresses produced from the tire/track vertical soil surface forces to produce the total vertical stress at a subsurface point.

Turning vehicles add even more complexity to the vehicle/terrain interaction model. For wheeled vehicles, the forces include the static weight, plus any dynamic weight (due to weight shift), plus increased longitudinal forces (vehicle rolling resistance increases with turning) producing wheel slip, plus centrifugal (lateral) forces due to the turning radius and velocity, plus any forces produced as non-turning wheels or tracks are dragged across the soil surface. The lateral movement of the wheels of a turning vehicle, and the slip occurring in the longitudinal direction will produce shear stress, and cause shear displacement of the soil. A study of the relationship between shear stress and shear displacement of soils is necessary to understand both the terrain deformation and the required energy and power. Wong (2001) indicated that there are three types of relationship between shear stress and shear displacement. The variation of strain-stress relationship was caused by the soil type, moisture content, and bulk density of soils. A physics-based shear stress-displacement model was proposed by Janosi and Hanamoto (Wong, 2001) :

$$\tau = \tau_{\max} \cdot \left(1 - e^{-j/K}\right) = \left(c + \sigma \cdot \tan\phi\right) \cdot \left(1 - e^{-j/K}\right) \tag{13}$$

where τ is the shear stress, j is the shear displacement, c is the internal cohesion of the soil, ϕ is the angle of internal friction of the soil and K is defined as the shear deformation modulus. For turning wheeled vehicles, the lateral shear stress resulting from the centrifugal force produces an applied shear displacement. The shear force multiplied by the shear displacement results in the shearing energy for the turning vehicle. For a turning tracked vehicle, the track slides back and forth a significant amount. This track slide will produce lateral soil displacement. Equation (13) can then be applied to determine the resulting lateral forces. The power can be calculated from the force, displacement and time in the same way as the vertical power was defined in Eq. (10).

There is a tremendous loss of energy to produce large amounts of soil deformation and relocation. In addition, during a turn the outside wheel slips and the inside wheel is being dragged forward; thus the power required for operating a turning wheeled or tracked vehicle is significant. The authors have conducted extensive research involving the rutting (both depth and width) resulting from turning wheeled and tracked vehicles. Different ruts are formed by the inside and outside track/tire. Soil piling during turning can affect the vertical profile of the terrain. In addition to the shear displacement resulting at the track shoe/soil interface, any sinkage will create a bulldozing effect that pushes the soil to form outside piles on both sides of the tire/track. The bulldozing forces can be modeled using the Passive Lateral Earth Pressure calculations, as shown in Figure 3. The forces resisting bulldozing are the weight of the soil and the shear forces along a defined failure plan. To simplify calculations, negligible friction between the soil and the tire/track interface can be assumed, resulting in a straight failure plane between the bottom of the tire/track and the soil surface. The angle of failure plane is 45 - ϕ/2.

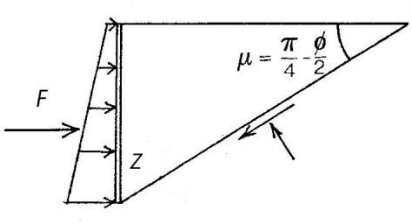

Figure 3 Force/deformation relationship on a turning wheel or track due to bulldozing

The total force at failure of a sunken tire/track shearing and displacing a soil wedge is defined as

$$F = b(\tfrac{1}{2}\gamma Z^2 N_\varphi + 2cZ\sqrt{N_\varphi}) \tag{14}$$

Where F is the bulldozing force at failure, γ is the soil unit weight, b is the width of the element, and

$$N_\varphi = \tan^2(45 + \varphi/2) \tag{15}$$

So to determine the bulldozing force at soil failure, the soil strength parameters, soil density, sinkage and width of contact are needed. If the bulldozing lateral displacement is known, then the bulldozing force is reduced by $(1 - e^{-j/k})$, where j is the shear displacement and k is the shear deformation modulus. It should be noted that as the tire/track sinks, Z increases and the bulldozing force also increases.

IMPLEMENTATION OF SOIL MODELS

At each time step, the state variables of the vehicle model will be passed to the VTIM, where they will be used in the tire model to determine the points of contact with the terrain surface. Once the kinematic contact points are determined, the tire model radial forces can be determined using Eq. (2), and the points in contact with the terrain can be decomposed into normal and tangential forces by utilizing the terrain surface normal information contained in the database. Each force can be used to find a subsoil pressure distribution by using the modified Boussinesq and Cerruti models, Eq. (5) and (12), respectively. For N tire-terrain contact nodes, a total of $2N$ pressure volumes will be calculated, one each for the normal and tangential force components.

The tangential forces produced by slip between the tire and the terrain are calculated on the surface of the soil using Eq. (13). If the vehicle is turning, an additional tangential force from bulldozing is calculated using Eq. (14). Combining the calculated tangential forces with the displacement of the soil allows for the calculation of energy/power required for the horizontal soil displacement. The energy and power required for both the vertical and horizontal soil deformation constitute the total extra energy required by the vehicle to operate on the deformable soil. A flowchart of the calculations performed for each time step in the VTIM is shown in Figure 4.

A given point in the soil volume that is affected by the tire contact pressure will have a total vertical pressure applied to it by superimposing the contributions of all the vertical subsoil pressures affecting that point, according to Boussinesq and Cerruti equations. The soil in the terrain volume is discretized into a three-dimensional grid of rectangles, where the horizontal dimensions are a function of the underlying geometry query routines and the depth is a tunable parameter depending on the desired fidelity of the soil mechanics calculations. Thus the soil point becomes a volume, and the vertical pressure applied at the top of the element can be used in conjunction with the current state of the volume of soil to calculate the change in soil density, Eq. (7), and vertical sinkage, Eq. (8). If the soil volume is currently undergoing compression, then the required energy and power are calculated with Eqs. (9) and (10). If the soil volume is currently undergoing rebound, only the change in vertical sinkage and soil density are computed.

The number of calculations required to determine and update the soil node states is large and can be determined as follows. Assuming a predetermined volume, $V = L*W*D$, with length L, width W and depth D, of terrain nodes that includes the soil that will be affected by the tire loading (i.e., an area slightly larger than the tire footprint, and a depth of no more than 2 feet) , a total of $2NV$, or $2NLWD$ summations are required to determine the vertical pressure on each terrain node affected by the surface load. Furthermore, LWD soil-mechanics calculations are required. Taking into account that the spacing between the terrain nodes that describe the surface

is small (to take into account high-frequency content of the terrain profile), a huge number of calculations are required to update the soil states due to a tire load at each timestep.

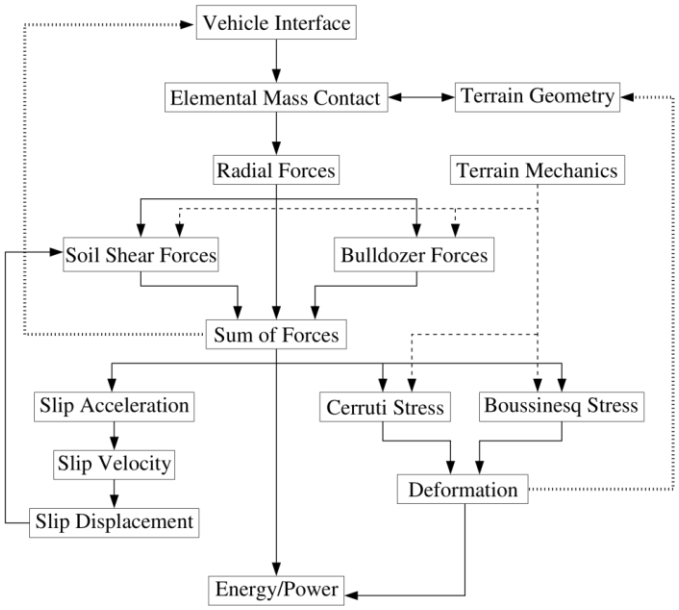

Figure 4 Calculation Flowchart

OPPORTUNITIES FOR PARALLELISM

Due to the nature of the equations above, it can be seen that the terrain geometry is spatially independent – that is, the terrain in one area does not depend upon that in another. The same is true for the individual tire elements. This means that calculations on different areas of the terrain and different elements of the tire can be embarrassingly parallel – it does not matter when (or where) the calculations for each area are performed, as long as they are all finished before moving on to the next set of calculations. This type of Single Instruction, Multiple Data (SIMD) problem maps perfectly to the GPU (Graphics Processing Unit) which can typically have hundreds of processors doing the same calculations on different sets of data in parallel.

For example, given a 12 inch wide, 36 inch diameter tire, and assuming a 0.2 inch nodal resolution in each direction, there can be up to 10,800 nodes for which the tire model needs to be directly applied to. Additionally, there are at least that number of nodes on the terrain for which the soil model must be applied (depending on how many layers of terrain nodes are used). At each time step in the simulation, none of the calculations within each model depend on each other, allowing them to be performed in parallel.

As mentioned above, SIMD problems map perfectly to the GPU in that the GPU is most efficient when all of its hundreds of processors are working on the same calculation, albeit using different data. However, one issue with the GPU (and most types of processors, for that matter) is that it can quickly become data starved – it processes the data much faster than it can send and receive it. Nvidia GPUs are designed in such a way so as to side step this issue. They have a dedicated copy engine for moving data to and from memory, thereby allowing the main processors to focus on calculations and not on moving data. As long as the main processors are sufficiently over-subscribed (that is, there are thousands or tens of thousands of calculations/threads waiting to be performed), the latency of copying data will be hidden as the processors are never idle while waiting for new data. While this architecture can (and is) be applied to CPUs as well, the GPU still has the advantage in that its memory bandwidth is approximately five times that of a typical CPU (120GB/s for a Nvidia Tesla C2070 compared to 20GB/s for an Intel Xeon E5520). Figure 5 shows approximate bandwidth speeds for moving data between different parts of a computer. It can also be seen that it is desirable to move as little data as possible between the CPU and GPU (co-processor) due to the inherent latencies of the PCI-e 2.0 system bus which connects the system memory on the CPU to the device memory on the GPU.

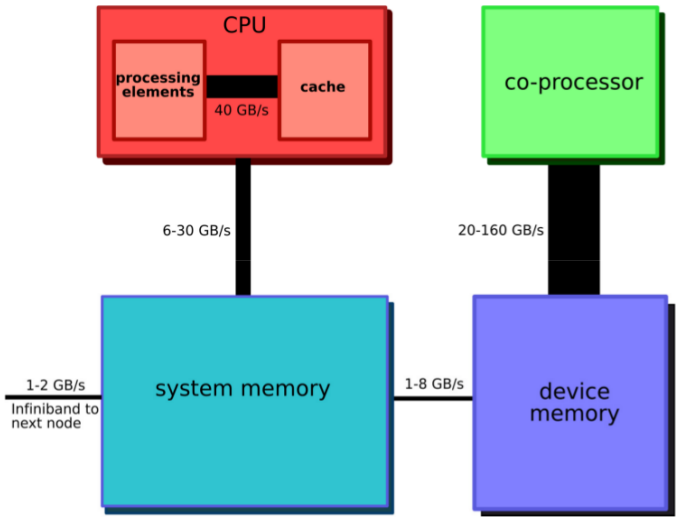

Figure 5 Bandwidth speed comparison

The MapReduce framework/methodology is used to process this large amount of data. MapReduce is a software methodology introduced by Google and inspired by the map and reduce functions from funtional programming that defines the workflow for processing large amounts of data quickly using multiple processors working in parallel. The map section of the method splits the input data set so that it is evenly distributed across all the processors. Each processor then applies any user-defined functions to the dataset in parallel and then passes the results back into memory. The reduce section of the algorithm is then applied to this set of results in order to get the final desired result. This section could, for example, add up all values calculated previously, sort them, and/or find all unique values.

One of the most common functions performed by the VTI is querying the data stored for multiple points of the terrain. In order to reduce the latency for copying data from memory to the processors, multiple points are grouped together and copied to the processors in one large chunk. This process is performed as follows: first, the list of all points required is assembled on the GPU and evenly distributed to each GPU processor. Each processor will then apply a basic spatial hashing function to each element. A reduction algorithm is then applied to these hashes to remove any duplicates. All the data for each of these unique hashes is then copied to the processors for use in the next step. It should be noted that this process will bring in data for points that were not directly queried. This is actually desirable because there is a strong likelihood that the extra data for those points will soon be required for future time steps. Thanks to the multiple layers of cache in the GPU, this data will then be readily available to the processors once they do need it, reducing or even eliminating the cost to copy it in from memory.

Once the terrain data has been loaded on to the GPU processors, the terramechanics functions can be applied. Again, since these functions may be applied on an independent, point-by-point basis, they may be performed in parallel on each of the GPU's scalar processors.

NUMERICAL EXPERIMENTS

An example of a test load being repeatedly applied to a single soil volume is presented. This example tests the response of the soil model to a directly applied load, and thus the calculation of subsoil stresses with the Cerruti and Boussinesq equations is not necessary. The applied normal stress to the soil node was calculated using data of a Stryker, operating in a CL soil at Ethan Allen Firing Range, traveling at a constant rate of 1.5, 3.0, and 6.0 m/s. As can be seen by Figure 6, the slower vehicle speeds increases the bulk density of the volume of soil at a greater rate initially; however, due to repeated loading, the rate of bulk density increase is lowered due to the increased density. This change of rate of increase is less apparent in the plot with the higher vehicle speed.

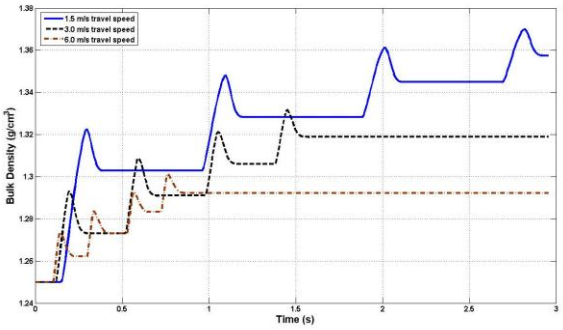

Figure 6 Bulk density and Applied stress as a function of time, 1.5 m/s (left) and 3.0 m/s (right) vehicle speed

The total vertical displacement, energy and peak power due to the deformation of the load applied by the Stryker moving at 1.5 m/s is shown in Figure 7. Notice that due to the effects of repeated loading, a majority of the energy required to deform the soil is accumulated from the first two applied loads. The total vertical displacement, energy and peak power attained for each of the three vehicle speeds is shown in Table 1. Although the peak power is nearly the same of all three vehicle speeds, the total energy and vertical displacement decrease as the vehicle speed increases. This is due to the reduced time that the vehicle load is applied, and also a result of the change in the rate of bulk density increase.

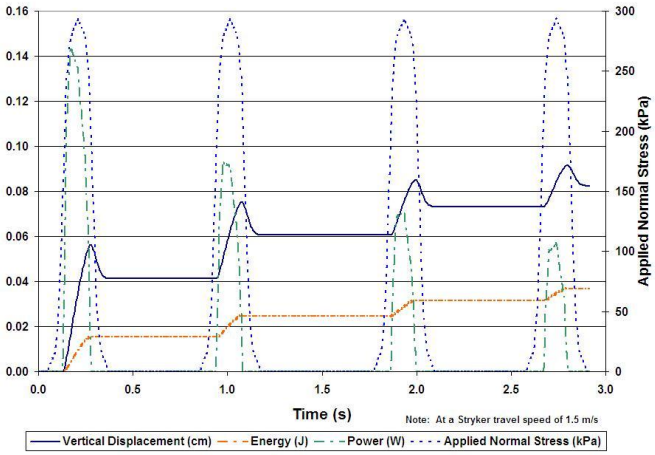

Figure 7 Vertical displacement, Power and Energy from vehicle speed of 1.5 m/s

In order to test the effect that the Boussinesq and Cerruti equations have when they are applied to the soil database, a tire normal force is applied which is the result of an applied vertical displacement on the wheel CG. A simplified tire model consisting of a set of radial springs applies a normal force on the surface of the terrain. Also, the following settings were used for the terrain mechanics settings of all soil nodes: an assumed Frolich stress concentration parameter of 3, an initial bulk density of 0.04515911 [lb/in^3], and σ_k = 20.356 [psi] was used for all soil nodes.

Table 1 Total vertical displacement, Energy and Peak Power from various vehicle speeds

Travel Speed [m/s]	Correct Total Element Vertical Displacement [cm]	Total Energy [J]	Peak Power [W]
1.5	0.095519	0.039816	0.180938
3.0	0.060483	0.031553	0.184590

6.0	0.033694	0.019222	0.186478

The following results are from the test simulation detailed in the above section, and are presented in the following order: soil column total vertical deformation, soil column energy to perform the deformation, and terrain surface profile. The maximum applied tire force and subsoil stress are listed in table 1 below, as well as the energy required to deform the soil node with the maximum subsoil stress value.

Table 2. Max tire force and subsoil stress at various steps

Step #	Max Tire Force [lb]	Max subsoil node Stress [psi]	Max Energy [lb-in]
0	621.7	505.8	6.93E-6
1	874.4	763.5	1.16E-5
2	1179.67	1134.1	1.89E-5
3	1559.1	1723.4	3.13E-5
4	1996.8	2476.9	4.83E-5
5	2476.9	3378.3	6.89E-5

The following plots show the sum of the deformation of the soil columns that are affected by the applied tire force. Figure 10 show the time evolution of the terrain due to the applied tire displacement. Figure 8 shows an isometric view of the accumulated vertical soil deformations. Notice that even though very large tire forces and subsoil stresses are applied in this test simulation, the time constant effect on the compressive loads prevents the soil deformation from instantaneously reaching the applied final deformation of 1", which would be seen in all the locations in Figure 1 near the contact patch. This is not the case, as shown in Figure 8 where the maximum soil deformation is less than 0.9".

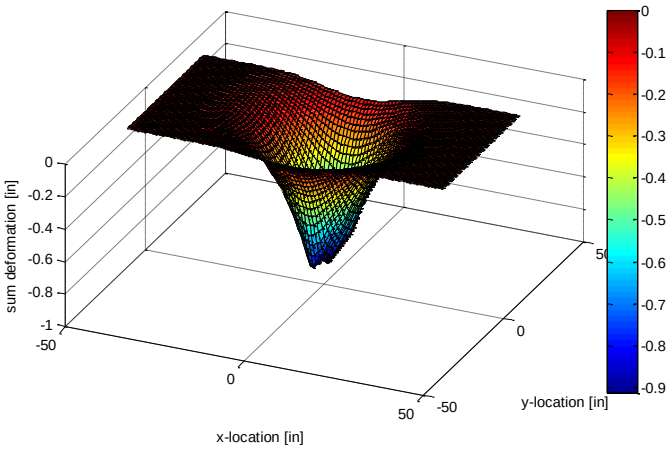

Figure 8 Total deformation, time step = 5, isometric view of surface plot

Figure 9 is similar to the plots above, except it shows the cumulative energy required to perform the deformations reported in the above plots.

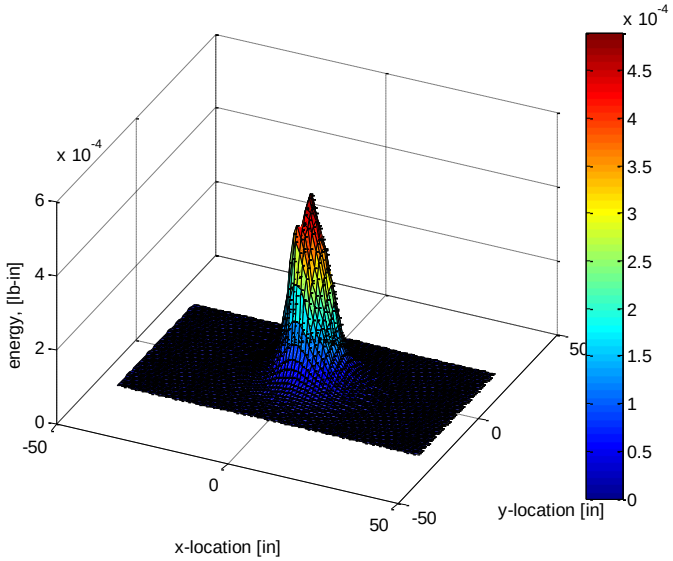

Figure 9 Total energy to perform deformation, time step = 5, isometric view

Figure 11 shows the terrain profile surface at the undisturbed configuration and after 5 steps are performed. Notice that the vertical deformation is in the shape of an ellipse around the tire contact patch when using the subsoil stresses to calculate bulk density change and sinkage, rather than having a shape identical to the contact patch, as is the case if the tire forces are applied directly to the calculation of bulk density change and sinkage. It should be noted that the propagation of subsoil stresses in the lateral and horizontal directions is reduced when a larger Frolich parameters is used, and would result in soil deformations that are more condensed around the contact patch.

SUMMARY/CONCLUSIONS

A physics-based tire and terrain model for use in off-road vehicle dynamics simulations has been developed and presented. The tire model is a simplified mass-spring-damper model, while the soil model consists of multiple components that model the vertical and lateral force/displacement relationships. The soil model captures the change in soil state in a volumetric sense, and does not make the assumption that the terrain remains homogenous in the vertical direction, which is what is typically done in most empirical terramechanics codes. Repeated loading and time-domain effects are taken into account, and the force/displacement soil equations can be utilized to calculate the required energy and power to deform the terrain. It is predicted that this model will result in not only more realistic mobility simulations, but also allow for a novel power and energy analysis technique for off-road vehicles.

Example numerical results verify that the soil model predicts the anticipated visco-elasto-plastic response to a repeated load, and that the calculations can be applied to a terrain database to produce similar results. This paper represents an ongoing effort between the University of Tennessee, University of Wisconsin-Madison, Mechsim, and the US Army TARDEC to incorporate the physics-based VTIM into a real-time vehicle dynamics simulator. As this is a work in progress, updated models and results from implementation will be reported at a later date. Experiments are planned to measure the driveshaft torque of a vehicle operating on deformable terrain as well as the end state of the disturbed terrain, and to validate the proposed models by comparing the experimental and simulation results for energy and power required to perform the soil deformation.

REFERENCES

1. Morrison, M., Romano, R., Reid, A., Gorsich, D., “High-Frequency Terrain Content and Surface Interactions for Off-Road Simulations,” SAE Paper 2004-01-2641, 2004.
2. Richmond, P., Jones, R., Creighton, D., Ahlvin, R., “Estimating Off-road Ground Contact Forces for a Real Time Motion Simulator,” SAE Paper 04TB-122, 2004.
3. Negrut, D. and J.S. Freeman (1994) “Dynamic tire modeling for application with vehicle simulations incorporating terrain,” SAE Paper No. 940223

4. Wong, J.Y. (2001) Theory of Ground Vehicles, 3rd edition. New York, NY: WILEY - INTERSCIENCE.
5. Koolen, A.J. and H. Kuipers (1983) Agricultural soil mechanics. Germany: Springer-Verlag.
6. Ayers, P. D. and J. Van Riper (1991) "Stress distribution under a uniformly loaded rectangular area in agricultural soils," *Trans. of the ASAE.* 34(3): 706-710.
7. Larson, W.E., S.C. Gupta, and R.A. Useche. (1980) "Compression of agricultural soils from eight soil orders," SOIL SCI. SOC. AM.J., 44: 450-457.
8. Feda, J. (1978) Stress in subsoil and methods of final settlement calculation. New York: Elsevier Science Publishing Co.

CONTACT INFORMATION

Dan Negrut, negrut at wisc.edu

Department of Mechanical Engineering, University of Wisconsin - MadisonAcknowledgments

APPENDIX

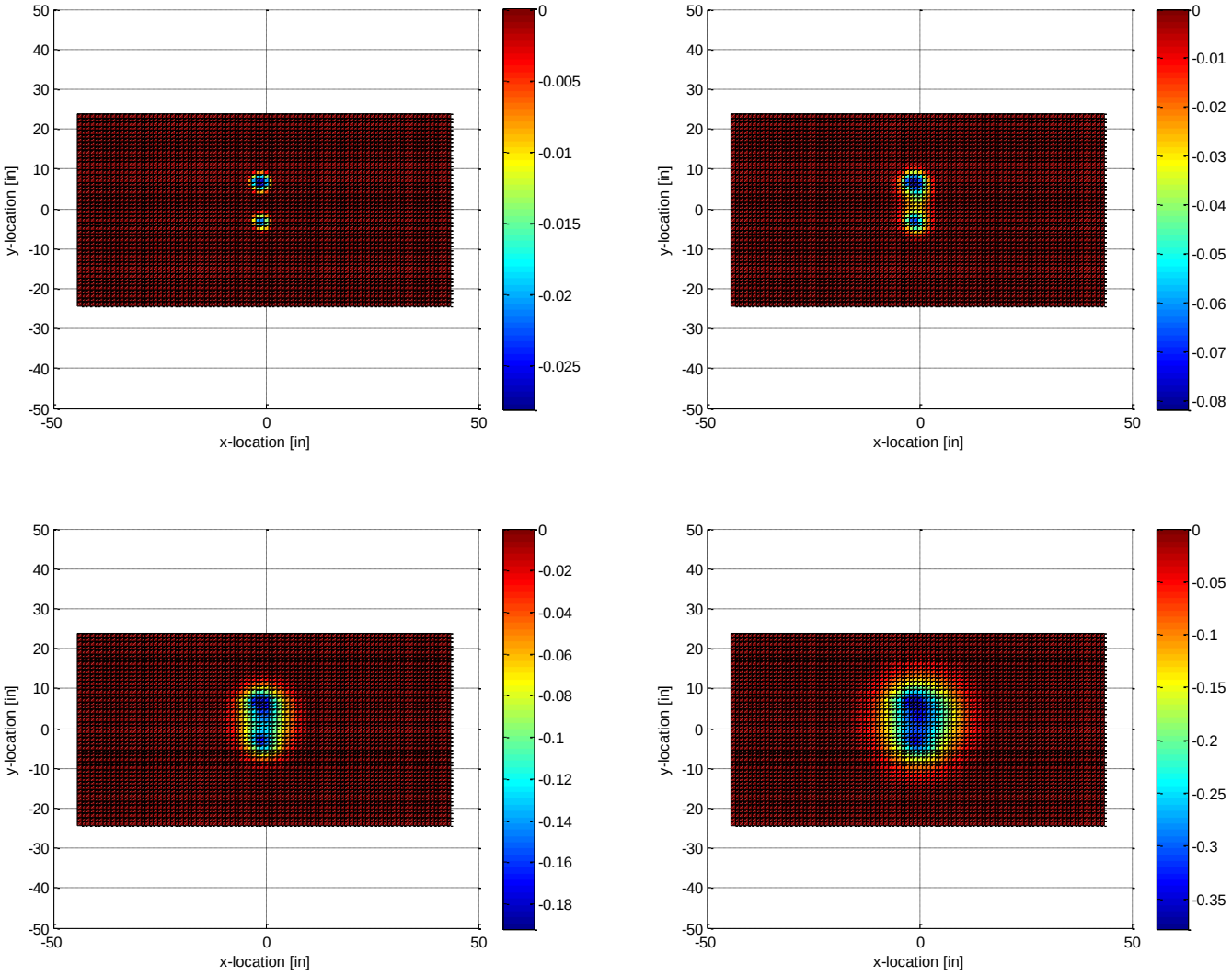

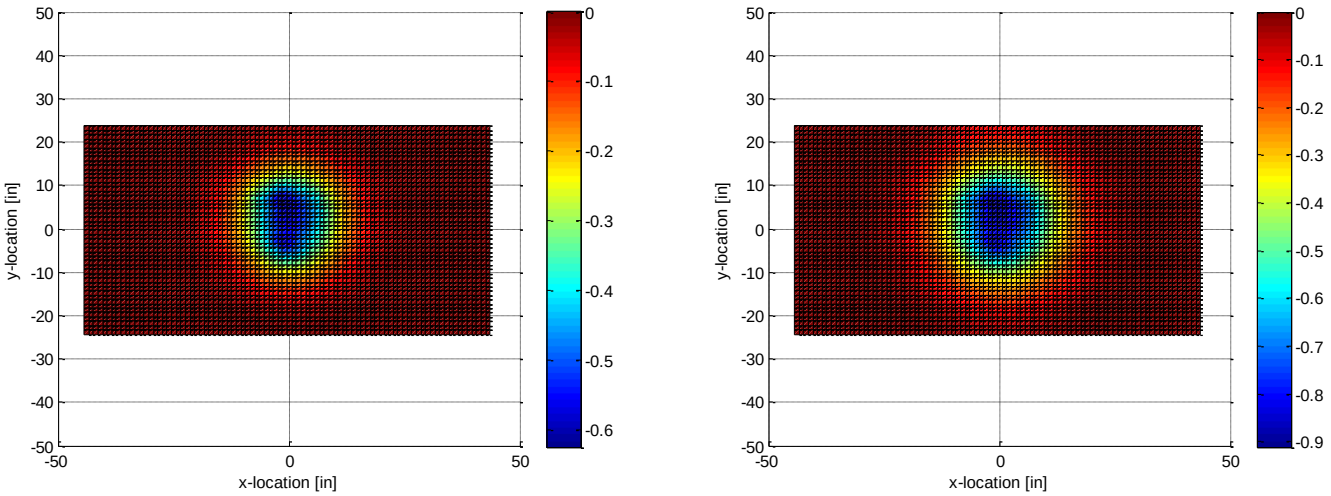

Figure 10 Cumulative soil deformation [in], steps 0 – 5, (top left to bottom right)

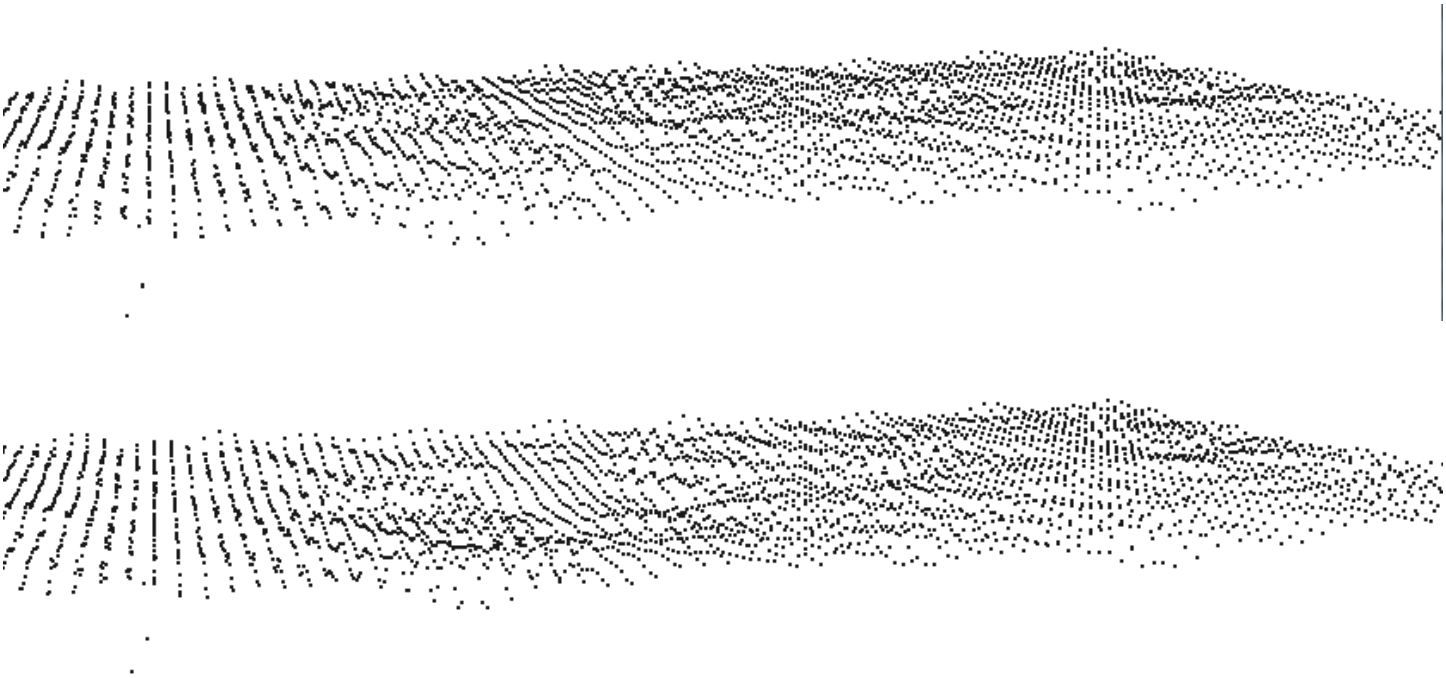

Figure 11 Undisturbed and final terrain profile